Impact of Battery Characteristics on PHEV Fuel Economy

Aymeric Rousseau, Neeraj Shidore, Richard Carlson, Dominik Karbowski
Argonne National Laboratory

Abstract

Plug-in hybrid electric vehicles (PHEVs) have the ability to drastically reduce petroleum use. The FreedomCAR Office of Vehicle Technology is developing a program to study the potential of this technology. This paper describes work in which several tools were used to evaluate the impacts of various parameters on PHEV fuel economy. First, the impacts of battery's energy and power were evaluated by using a global optimization algorithm. Then the impact of temperature was assessed by using two complementary approaches to evaluate battery hardware: simulation in an emulated vehicle system and actual vehicle testing.

1 Introduction

The most significant technical barrier to developing commercially viable plug-in hybrid electric vehicles (PHEVs) is the energy storage system. The challenge is to develop batteries that are able to meet both the requirements imposed by a PHEV system and market expectations of the system's cost and length of life. In this context, a vehicle systems approach is needed to investigate the operational requirements specific to PHEV technology. This paper describes work done to investigate the impacts of battery energy and power and of temperature on PHEV fuel economy. To achieve that goal, both hardware and software were employed.

Simulation was used to analyze the impacts of battery energy and power during ambient conditions. Both hardware and simulation were then used to assess the impact of battery temperature on the vehicle's all-electric range (AER). In that case, the battery hardware was evaluated within an emulated vehicle system. Because the models were developed for ambient temperatures, the impact of the battery alone could be analyzed. In this case, in order to maintain the fairness of the comparison, the high level vehicle control strategy was not modified. Finally, a vehicle was tested to evaluate the impact of temperature on all the powertrain components (not just the battery) in a blended mode approach.

2 Battery Energy and Power Impact

2.1 Modeling Assumptions

The configuration used to evaluate the impact of battery power and energy on PHEV battery use and energy consumption was a parallel pre-transmission, similar to the one used in the DaimlerChrysler Sprinter van [1] and the Mobile Advanced Technology Testbed (MATT) [2].

The base vehicle represented a small sport-utility vehicle (SUV) similar to a Toyota Rav4. It was powered by a 100-kW engine. The vehicle mass was 1710 kg without the battery and electric machines, whose sizes were variable. The electric machines data were based on the Toyota Prius MY04 motor. The batteries used in the study were scaled versions of the SAFT VL-41M. Vehicles were sized by using Argonne National Laboratory's Powertrain Systems Analysis Toolkit (PSAT).

Three different driving cycles were used: urban dynamometer driving schedule (UDDS), highway fuel economy driving schedule (HWFET), and LA92. The UDDS and HWFET are standard U.S. Environmental Protection Agency (EPA) cycles currently used for certification in the United States. LA92, also called the "unified cycle," is more aggressive and more representative of current driving habits. The distances used in this study were 10, 20, and 40 mi (16.1, 32.2, and 64.4 km, respectively).

After the components were sized by using PSAT, they were simulated by using a global optimization algorithm based on the Bellman optimality principle. The algorithm output the engine torque, motor torque, and gear number to achieve minimal fuel consumption. One of its main advantages is that the control logic was no longer an input of the simulation but an output, which ensured that each vehicle

was operated optimally, independent of it's the sizes of its components. Global optimization requires the knowledge of the cycle beforehand and results in an analytical tool that is precious to the control logic designer.

2.2 Optimal Control and Battery Use

PSAT was used to size the vehicle so that the battery was discharged from a 0.9 state of charge (SOC) to a 0.3 SOC when the vehicle was driven 20 mi on several iterations of the UDDS.

One run of the global optimization output resulted in various ΔSOCs. (The ΔSOC is the difference between the initial SOC, a value between 0.3 and 0.9, and the final SOC, which is always 0.3.) Figure 1(a) shows the variation in battery SOC over time when the vehicle was driven 20 mi on the UDDS for three ΔSOCs. The battery was fully discharged when the initial SOC was 0.9. If the initial SOC is identical to the final one, the vehicle is operated in a charge-sustaining (CS) mode, which is typical of a non-plug-in hybrid vehicle. When only half of the battery energy is discharged, there is not enough energy to complete the cycle in an electric vehicle (EV) mode. The vehicle then operates in a blended mode, during which the engine is used at judicious moments, generally at high loads and efficiency.

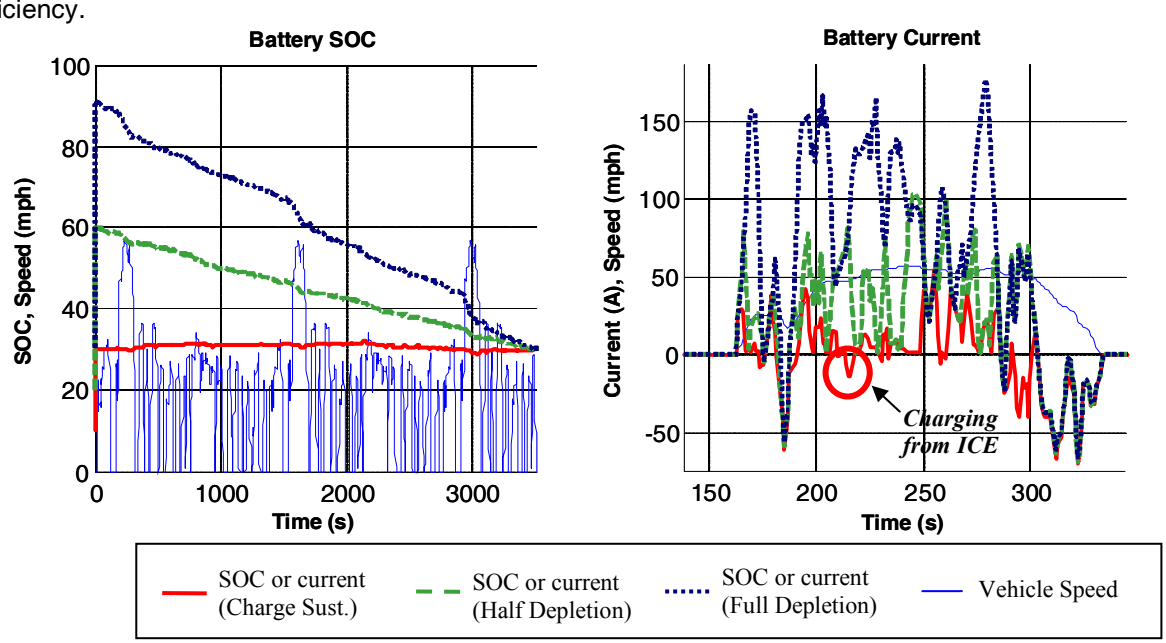

Figure 1: Battery use for different levels of discharge:
(a) SOC (UDDS, 20 mi); (b) current (UDDS, 20 mi, detail)

Figure 1(b) shows current levels in the three discharge scenarios during the second hill of the UDDS cycle. Although the regenerative events were identical, the battery current is higher than it was in EV-mode. The engine charges the battery at times when it is in a CS mode.

Another mode of representing global optimization data is to use ΔSOC (or any related parameter) for the abscissa. Each ΔSOC can be associated with the electric energy required to recharge the battery from its final SOC back to its initial one, using a 90%-efficient charger, and the distance travelled. Figures 2(a) and 2(b) depict the root mean square (RMS) current and fuel consumption versus electric consumption for various cycles and various distances driven. CS mode was achieved for 0 Wh/km. EV (or very close to EV) mode was achieved on the UDDS for slightly above 200 Wh/km. Blended mode was between those two values.

For a given cycle, fuel consumption and RMS current depend primarily on Wh/km (as do other control-related parameters) [3]. The more electric energy that is used per unit of distance, the less fuel is consumed, and the higher the RMS current is.

When comparing the RMS current for full discharge (ΔSOC = 0.6) and for no discharge, one notices that the RMS current increases from 26 to 60 A on the UDDS (39 to 75 A on the LA92). On the other hand, full discharge for a distance double the AER leads to 39 A on the UDDS and 55 A on the LA92.

If the same vehicle was driven on double the AER for 40 mi but in EV mode followed by CS mode, the first half of the trip would be done under an EV strategy, with an RMS current of 60 A on the UDDS (75 A on the LA92), and the second half would be done under CS mode, with an RMS current of 26 A on the UDDS (39 A on the LA92). Those results can be compared to the optimal control on that same 40-mi distance, which would result in an RMS current of 39 A on the UDDS (54 A on the LA92).

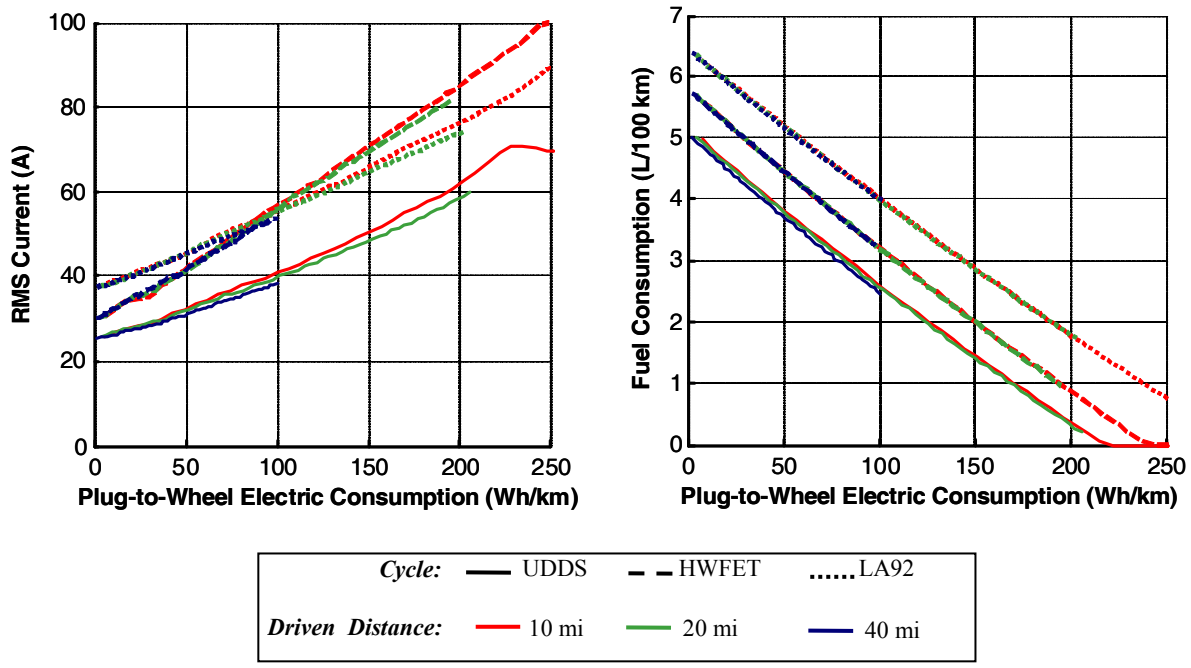

Figure 2: RMS current (a) and fuel consumption (b) vs. plug-to-wheel electric consumption
Various cycles are in different colors/shades); various distances driven are in different line styles. For example, a lighter shade/pink dotted line corresponds to 10 mi on LA92.

2.3 Battery Energy Impact

2.3.1 Vehicle Sizing

With the vehicle described in Section 3.1 as the base, an automated sizing procedure was used to generate five vehicles with various AERs. Battery power was defined to follow the UDDS speed trace up to 30% SOC. Battery energy was determined by the desired AER. The energy requirements affected the battery capacity while the bus voltage was maintained at 200 V. The main parameters are summarized in Table 1.

Table 1: Main parameters of various AER vehicles

AER (mi)	5	10	20	30	40
AER (km)	8.0	16.1	32.2	48.3	64.4
Vehicle mass (kg)	1808	1823	1852	1879	1911
Battery capacity (Ah)	12	23	45	66	90
Battery usable energy (kWh)	1.5	2.9	5.5	8.1	11.1
Battery power-to-energy ratio	30.3	15.7	8.2	5.6	4.1

As battery capacity increased with AER, the vehicle became heavier. However, because of the Li ion's high specific energy, the variation in mass was small –6% between the 5-mi-AER vehicle and the 40-mi-AER vehicle. As a result, battery pack power remained relatively constant at 75 kW.

2.3.2 Battery Use and Fuel Consumption

The least amount of fuel a vehicle can consume on a given cycle and distance is highly related to the battery energy, as shown in Figure 3. Higher battery energy means higher fuel displacement (i.e., more fuel is saved by the PHEV than a conventional car, whose input energy comes from fuel only). However, when the distance driven is below the AER, as it was for the 20-AER and 30-AER vehicles for 10 mi on UDDS, longer-range vehicles tend to be slightly penalized because of their higher mass.

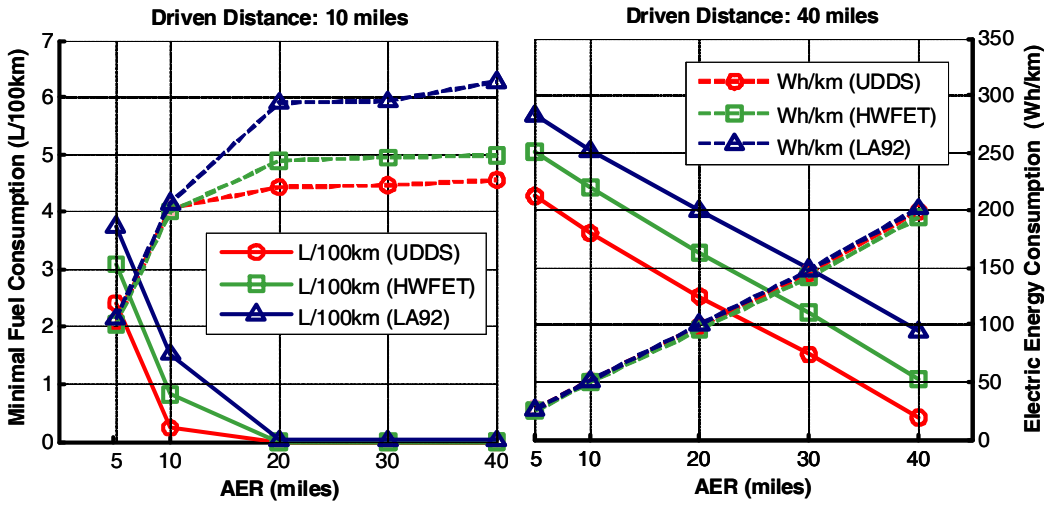

Figure 3: Minimal fuel consumption and associated electric energy consumption

Figure 4 shows that RMS current followed the same trend as electric consumption. When the AER was higher than the driven distance, the vehicles were driven in EV or EV-predominant mode, and RMS current was influenced by vehicle mass only. When the AER was below the driven distance, the RMS current increased proportionally to AER, since vehicles with higher AER used their battery more often.

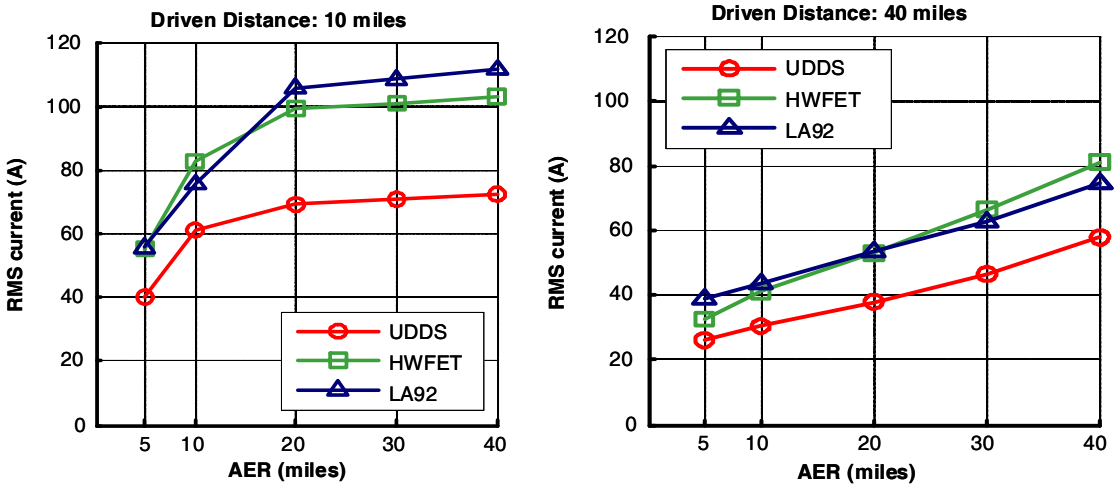

Figure 4: RMS current for strategies resulting in minimal fuel consumption

2.4 Battery Power Impact

2.4.1 Vehicle sizing

To evaluate the impact of electric system power sizing on energy consumption, the 10-AER vehicle was used as the base for defining vehicles that have a battery and electric machine that are 40% or 20% more or less powerful yet maintain the same energy. The main characteristics of those vehicles are summarized in Table 2.

Table 2: Main characteristics of various power ratios for vehicles

Power scaling ratio	0.6	0.8	1	1.2	1.4
Vehicle mass (kg)	1785	1804	1823	1842	1860
Battery maximal power at 30%SOC	45	60	75	89	104
Battery power-to-energy ratio (W/Wh)	9.4	12.5	15.6	18.8	21.9
0- to 60-mi per hour (mph) time(s)	8.6	7.8	7.3	6.8	6.4

2.4.2 Battery Use

Figure 5 shows minimal fuel consumption on several cycles for the same distance of 10 mi, as well as the electric energy consumption at which the minimum was reached. As the electric system power decreased, so did the ability of the vehicle to run in EV mode, which resulted in more use of the engine and increased fuel consumption. That increase was more significant when the cycle was aggressive as a result of the reduced rate at which regenerative braking energy was recuperated. Upsizing the electric components (power scaling ratios of 1.2 and 1.4) did not significantly change fuel consumption. On the other hand, downsized (power scaling ratios of 0.6 and 0.8) electric components had a greater impact and increased fuel consumption.

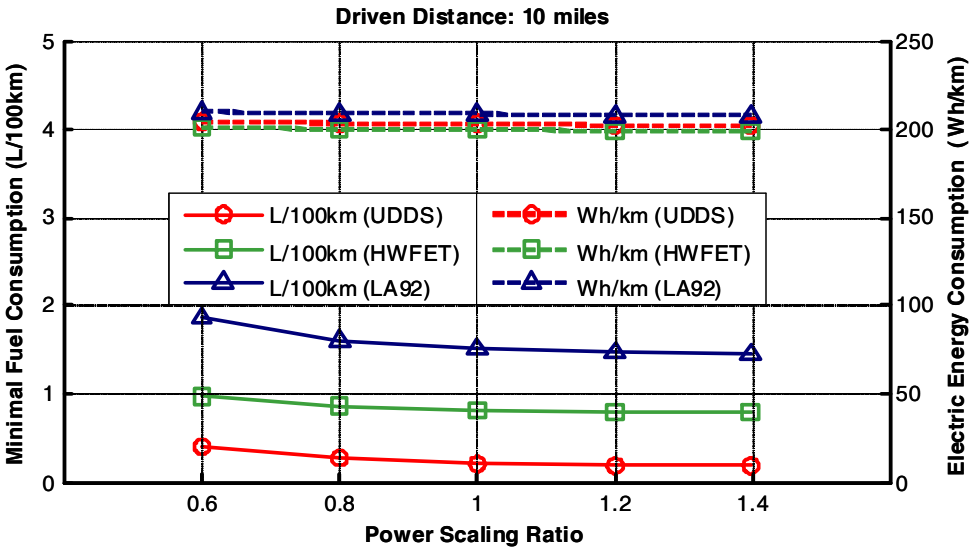

Figure 5: Minimal fuel consumption and associated electric consumption – distance driven: 10 mi

Battery power had little impact on RMS current, as shown in Figure 6, because of the limited occurrence of the very high power events. The LA92 was the only cycle on which there was an impact, because the braking events were more aggressive on this cycle than on the other cycles.

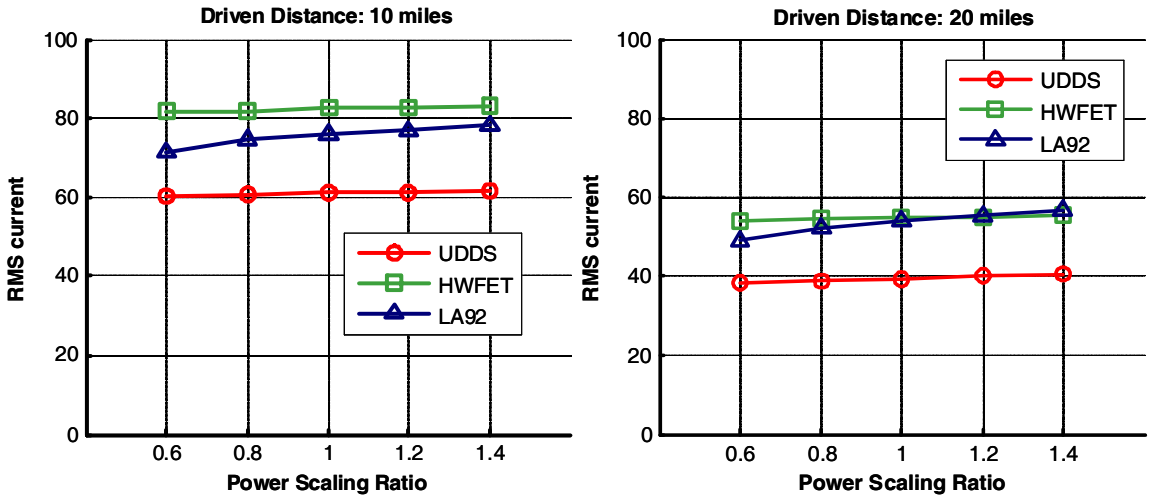

Figure 6: RMS current for strategies resulting in minimal fuel consumption

While the batteries operated at similar current levels, independently of their power, they did not operate in the same "power zone." The battery used for this study had a continuous maximum current as well as a higher 10-s maximum current. The global optimization algorithm used only the latter as the battery power limit. We could therefore define a "red zone," in which the current was between those limits. Figure 7 shows that lowering the power resulted in a more aggressive use of the battery: 45% of current was in the so-called red zone when a vehicle with 60% of the original power was driven 10 mi on the LA92, up from 9% for the original power. When the vehicle was driven a longer distance, the red-zone operations were reduced. Indeed, the same battery energy was discharged for twice the distance and in twice the time, which means it was discharged more evenly throughout the cycle, letting the engine run at high road loads.

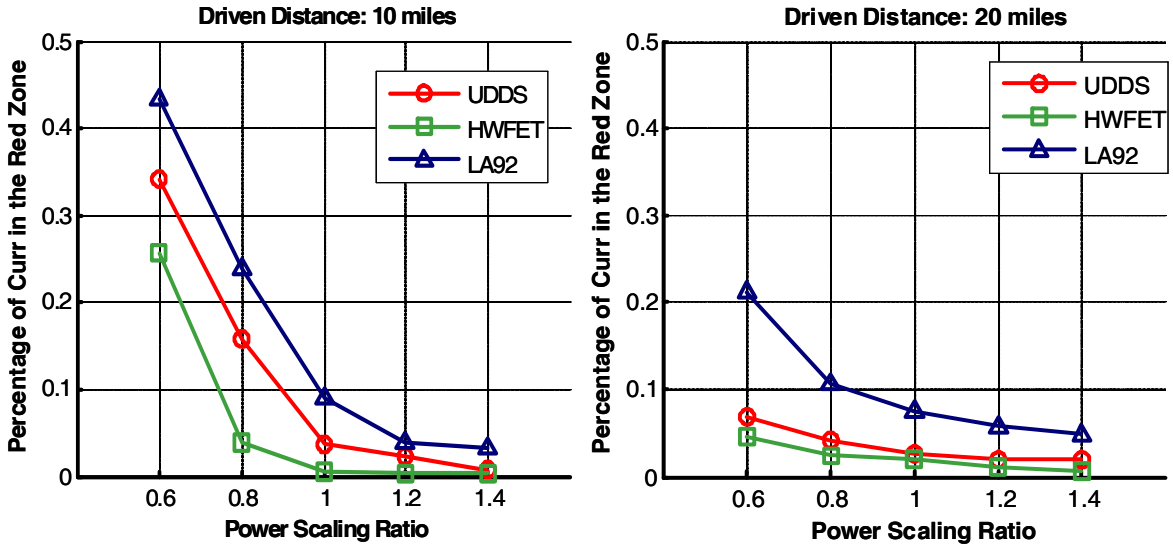

Figure 7: Percentage of current in the red zone of the battery for minimal fuel consumption

3 Battery Temperature Impact

3.1 Temperature Impact with Constant Vehicle Control Strategy

3.1.1 Experiment description

For this experiment, a battery pack was evaluated in an emulated vehicle system context [4]. The rest of the vehicle was emulated by PSAT models and controlled through a direct-current (DC) power supply. The battery hardware used is described in Table 3

Table 3: SAFT-JCS VL41M specifications

Parameter	Value
Capacity	41 Ah at C/3
Operating voltage	194.4 to 288 V
Continuous current	150 A continuous for 30 s at 30°C
Discharge power	61 kW for 30 s at 50% SOC at 30°C

At low (subzero) temperatures, the energy delivered by the battery to the PHEV was significantly reduced, resulting in a lower AER. This result occurred because there was a decrease in the inherent capacity of the battery at low temperatures and an increase in the internal resistance. The objective of the experiment was to quantify the impact of a cold battery on the AER of a PHEV. Since the vehicle was emulated and the models did not account for temperature effects, the AER variation was due solely to the battery. While several methods to actively heat up the battery are possible and would probably be used in vehicles, increasing the battery temperature by using its own heat loss was used here as a baseline case against which all other methods could be compared.

The battery was tested at different temperatures (–7°C, 0°C, and 20°C). The battery was cooled down to low temperatures by circulating coolant through it. The battery cells were surrounded by the coolant water jacket so the cells were exposed only to the cold temperature of the coolant water/bladder and not to the normal ambient temperature of the lab in which the test stand/battery was situated. The VL41M battery, being a prototype for test bench applications, had a steel casing that was roughly 1/4-in. thick, which housed the modules, coolant loop, battery management system (BMS), and other safety and monitoring devices. Because of this design and the fact that the battery was surrounded by the coolant jacket, one could assume that the impact of the external ambient temperature on the cells would be negligible.

To quantify the impact of temperature, the virtual vehicle was subjected to consecutive urban cycles from an initial SOC of 90% until a 30% SOC was reached. For the cold case (–7°C and 0°C), active cooling of the battery was stopped as soon as the test started, since experimenters wanted the battery temperature to rise as fast as possible to eliminate restrictions on battery charge/discharge power at cold temperatures. In the 20°C case, the battery coolant was constantly circulated through the battery to maintain the temperature. (For the –7°C and 0°C cold case, the temperatures were those of the coldest modules of the battery; other modules were within 5°C of this temperature.) Table 4 provides some specifications on the virtual vehicle used for the experiment.

Table 4: Specifications of the virtual vehicle

Vehicle configuration and class	Pre-transmission parallel, SUV
Vehicle mass	2049 kg
Vehicle battery	JCS SAFT -VL41M
Transmission	Five-speed manual
Vehicle coefficient of drag, frontal area	0.41, 2.88 m^2

3.1.2 Results

Figure 8 shows the SOC versus time for the three initial temperature conditions. As expected, the battery discharged quicker at lower temperatures, resulting in a lower EV range.

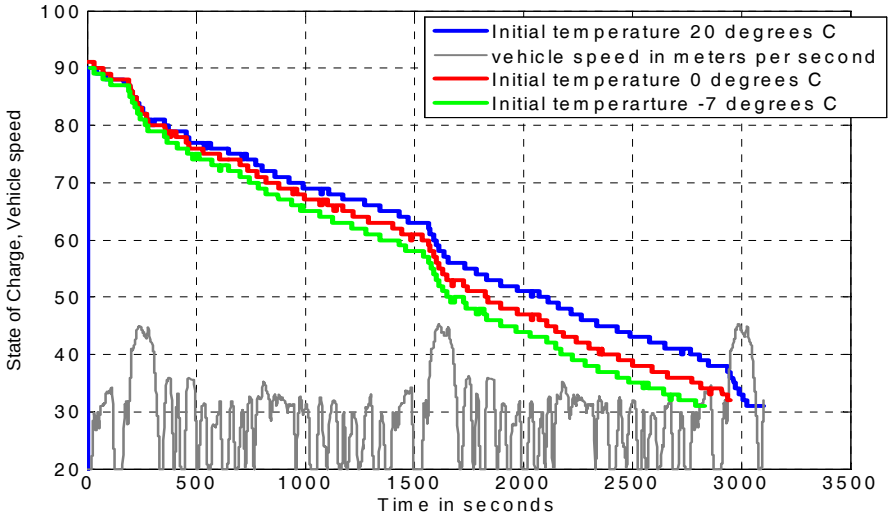

Figure 8: Decrease in SOC for the three initial temperatures

Figure 9 shows the decrease in AER with a decrease in initial temperature. Compared to the reference temperature (20°C), the AER decreased by 9% at 0°C and 13% at –7°C. Figure 12 shows the rise in battery temperature for the different initial conditions. As expected, the battery heated up quickly for colder initial temperatures. The resolution for the temperature was 1°C.

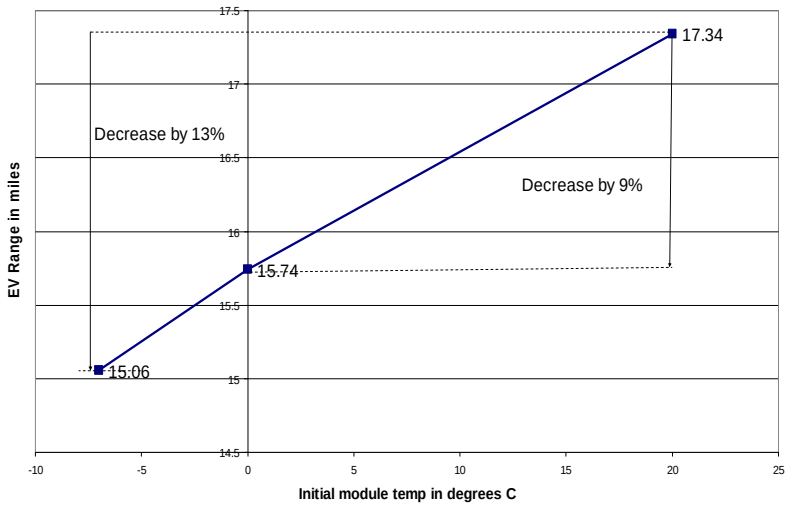

Figure 9: Decrease in EV range with decrease in temperature; percentage decrease in EV range

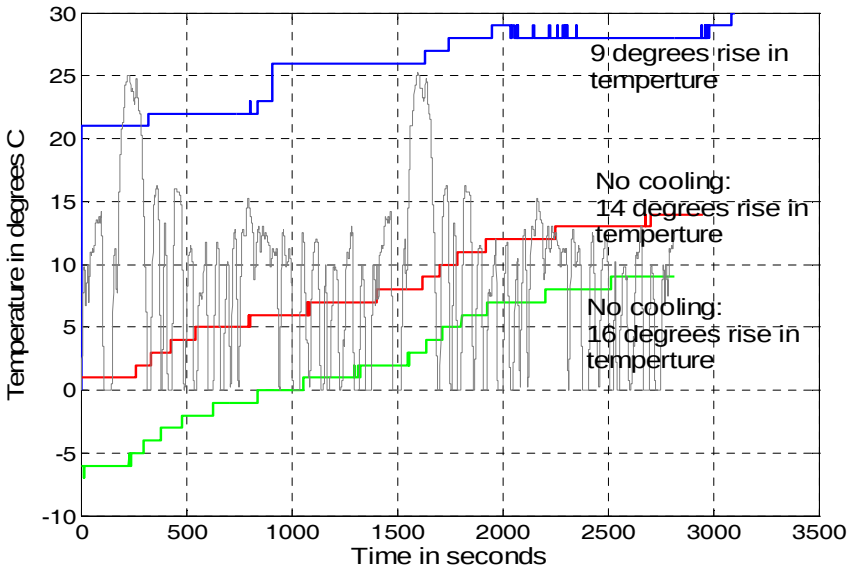

Figure 10: Increase in battery temperature for the three initial temperature cases

3.1.3 Analysis

The reduction in battery energy resulting in lower AER could be attributed to several causes:

1. Restrictions on battery usage (regen and propulsion) at low temperatures, which resulted in less regen energy being captured by the battery;
2. Increased internal resistance; and
3. Other losses. (For the test setup, the battery voltage and current were externally measured at the battery terminals. It was not possible for the instruments to measure the inherent decrease in battery capacity due to low temperature. All such factors that could not be measured were categorized as “other losses” for this analysis.)

Therefore,the loss in energy delivered by the battery could be described by Equation 1. Equation 2 describes the other losses that were calculated from Equation 1.

$$\Delta kWh = \Delta I^2Rt + \Delta Regen\ Energy + \Delta Other\ Losses \quad (1)$$

$$\Delta Other\ Losses = \Delta kWh - \Delta I^2Rt + \Delta Regen\ Energy \quad (2)$$

where

ΔkWh = difference in energy delivered by the battery at 20C case and at colder temperature (–7°C or 0°C) case.

ΔI^2Rt = difference (increase) in the heat energy lost due to the increase in the internal resistance with temperature.

$\Delta Regen\ Energy$ = difference in the regenerative energy captured at 20C case and the regenerative energy captured at lower temperatures (–7C or 0C) case.

The ΔkWh for different initial temperatures is shown in Table 5.

Table 5: kWh delivered by the battery for different initial temperatures

Initial Temperature	Battery kWh	ΔkWh
20	6.2	0
0	5.6	0.6
–7	5.5	0.7

ΔI^2Rt between the 20C case and the 0C and –7C case were calculated by subtracting the I^2Rt losses at 20C from the I^2Rt losses at 0C and –7C, respectively. Resistance values were estimated by plotting V,I plots for each SOC. Δ *Regen Energy* between the 20C case and the 0C and –7C case were calculated by subtracting the *Regen Energy* captured at 20C from the *Regen Energy* at 0C and at –7C, respectively.

The other losses were then calculated by using Equation 2. Table 6 lists the contribution of each kind of loss toward reduction in the total energy delivered by the battery. From Table 6, the following observations could be made:

1. The decrease in battery capacity at low temperature was the major cause for the decrease in battery energy delivered to the vehicle.
2. A large part of the decrease in energy delivered to the vehicle at low temperatures was due to the battery regenerative power limitations (34%). This decrease remained constant for both temperatures because of the controller.
3. The increase in ΔI^2Rt losses (12% at –7C and 8% at 0C) was due to the higher battery resistance at low temperatures.

Table 4: Percentage contribution of each loss toward the decrease in kWH delivered by the battery

Initial Temperature	ΔWh compared to Wh delivered at 20°C	$\Delta Regen\ Energy$ as % of ΔWh	ΔI^2Rt as % of ΔWh	$\Delta Other\ Losses$ as % of ΔW
0C	530	34%	8%	58%
–7C	730	34%	12%	54%

Except for the decrease in battery energy delivered as a result of the decrease in battery capacity, all factors ($\Delta Regen\ Energy$, ΔI^2Rt) were subject to the drive cycle used for the virtual vehicle and the method of battery warm-up.

3.2 Temperature Impact with Variable Vehicle Control Strategy

3.2.1 Vehicle Description

The Hymotion Escape PHEV (Figure 11) testing was conducted in subfreezing temperatures to determine the impact of battery performance on fuel consumption. In subfreezing temperatures, all components were less efficient.

Figure 11: Hymotion Escape PHEV

The Hymotion Escape PHEV is a conversion from a Ford Escape hybrid. The vehicle uses the Ford Escape NiMH battery system and adds in parallel an additional 7-kWh Li-ion battery system that uses A123 Li-ion cells. An actively controlled DC-DC converter provides power from the Li-ion battery system to the hybrid high-voltage bus to enable charge depletion operation. Figure 12 shows a schematic of the Hymotion battery system and its connection to the Escape powertrain.

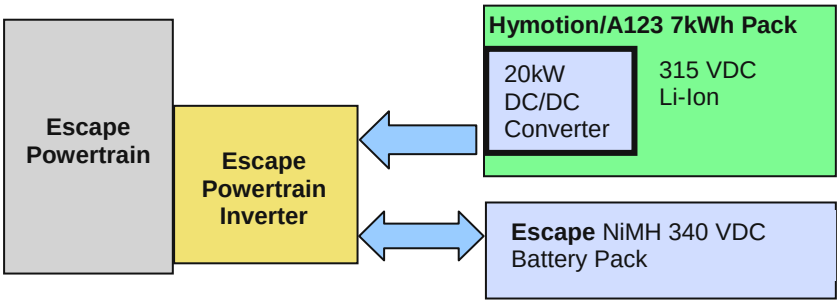

Figure 12: Hymotion Escape PHEV battery system schematic

3.2.2 Experiment Description

On-road testing was conducted during subfreezing conditions. The vehicle was allowed to cold soak outside for more than 12 hours before testing to allow the entire vehicle to reach or approach a steady-state temperature. The driving test cycle, called the ANL city cycle, was similar to the UDDS city cycle. Typical speeds were 30 mph, and accelerations were mild. Each cycle was 3.3 mi long and lasted 10 minutes. The cycle was repeated six times to provide enough time and distance for all of the vehicle systems to approach or reach a steady-state operating temperature. Because this on-road driving cycle had been used previously and found to have good repeatability [5], it was felt that it would provide good experimental results.

A CAN bus data acquisition system was used to record several dozen parameters at 10 Hz. The channels included current, voltage, temperatures, vehicle speed, and engine speed. Fuel economy and distance traveled were manually recorded from the dashboard display throughout the testing.

3.2.3 Results

Two tests were conducted to isolate the effect of battery temperature on fuel consumption. The first test was conducted after the vehicle cold soaked at –5°C overnight (>12 hours). The powertrain, driveline, and battery system temperatures were all –5°C (+/–2°C) at the beginning of the test. The results of this test are shown in Figure 13. The fuel economy increased rapidly at the beginning of the test and asymptotically approached steady state near the end of the 20-mi Argonne city cycle driving loop. The engine coolant temperature reached steady-state operating temperature after about 3.5 mi of driving, whereas the battery temperatures were still rising at the end of the 1-hour test.

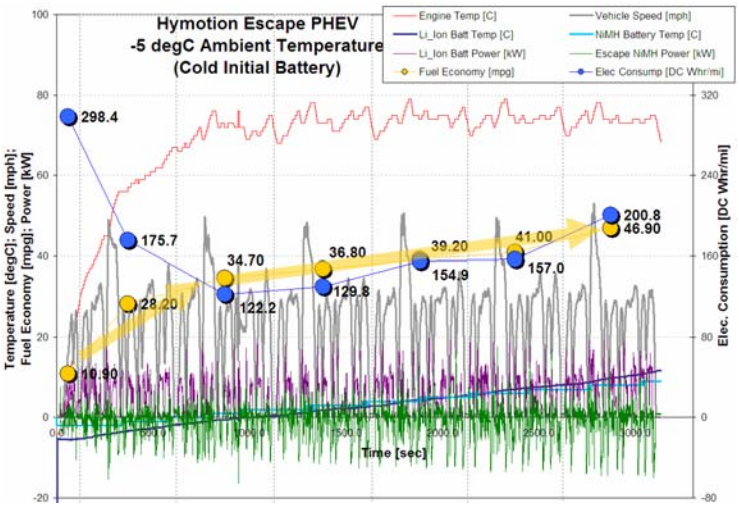

Figure 13: On-road test in which entire vehicle was cold soaked before testing

For the second test, the battery systems were warmed to a target temperature of 20°C while the rest of the vehicle cold soaked at the ambient –5°C. The warming was accomplished by a small heater that warmed both batteries. The results from this second experiment are shown in Figure 14. The NiMH Escape battery began the test at 10°C, whereas the Hymotion Li-ion battery system was warmer than 20°C. Again, the powertrain began the test at –5°C. The fuel economy nearly reached steady state after only 3.5 miles, and the fuel economy closely tracked with the engine temperature. This result occurred because the engine efficiency was greatly increased at higher temperatures. The continued slight increase in fuel economy occurred because the rest of the powertrain and driveline continued to warm up, which further reduced powertrain losses.

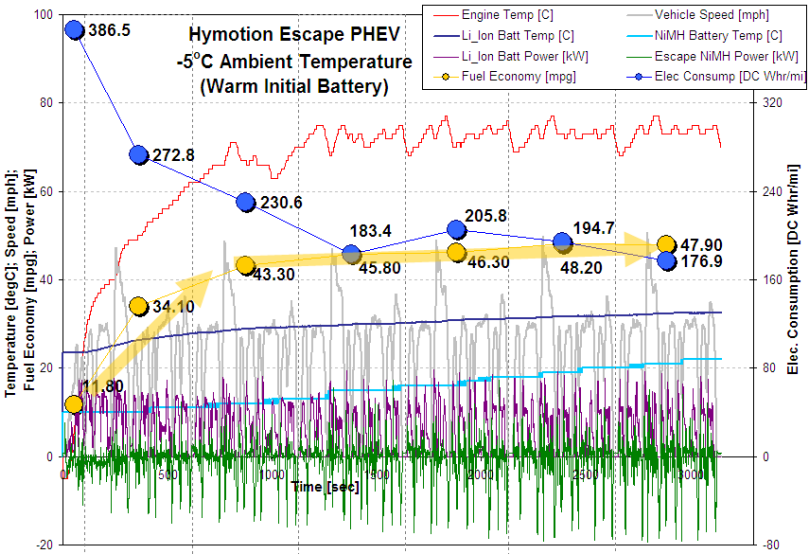

Figure 14: Batteries were warmed before testing while the vehicle cold soaked at -5°C

The difference between these two tests showed the impact of battery temperature on fuel consumption at subfreezing temperatures. For an ambient temperature of –5°C, the steady-state fuel economy was roughly 48 mpg, and the electrical energy consumption was 190 Wh/mi. The engine on/off operation was nearly the same for the two tests, but the electrical energy consumption was quite different. This might have occurred because the production battery calibration in the Escape powertrain control system could not be changed or modified by the Hymotion system. In the first test with the initially cold batteries, the energy provided by the Hymotion battery system was less in the second, third, and fourth cycle than it was in the first cycle. This result shows that the Li-ion battery system could provide a considerable amount of power at cold temperatures, but this situation occurs because the control parameters and calibrations could not be modified; therefore, the Li-ion cold-temperature power advantage could not be fully utilized.

To fully quantify the fuel economy impact of the temperature of the battery system as compared to the impact of the powertrain and driveline warm-up, Figure 15 shows the percent increase in fuel consumption over steady-state fuel consumption (48 mpg) at –5°C. For the first cycle, the overall increased fuel consumption was 70%. The powertrain's and driveline's reduced efficiency accounted for 41%, as shown in red, and the battery system accounted for the remaining 29%, shown in blue. As the engine quickly warmed up, the fuel consumption impact rapidly decreased. Once the engine was at steady-state operating temperature, the transmission and driveline caused the remaining fuel consumption impact. The rise in the battery system's temperature was fairly slow, which made the fuel consumption impact from the battery temperature taper off over a much longer time.

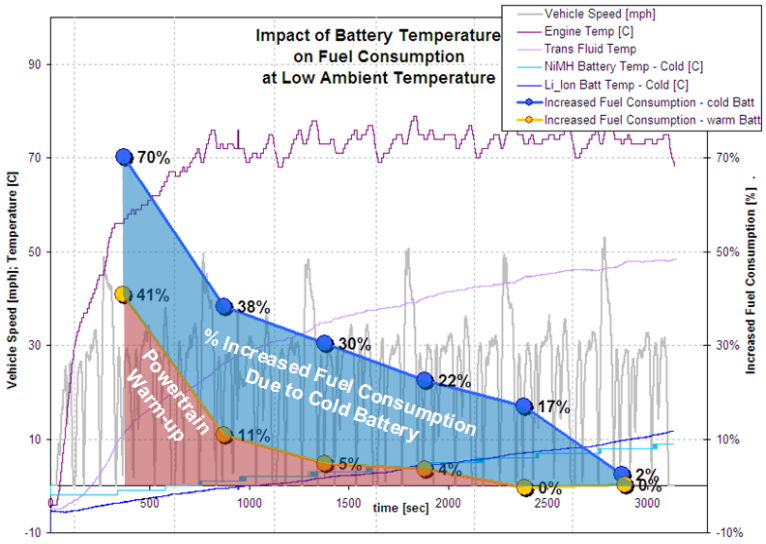

Figure 15: Fuel consumption differences between the two tests

Figure 16 shows the difference in the energy of the battery system for both propulsion and regenerative braking. The rate of battery energy out (propulsion) differed until the last cycle. Since the Hymotion system only output power, the regenerative braking energy difference was solely from the NiMH battery.

This Escape PHEV conversion driven on an urban route shows the quality of the A123 Li-ion technology used in the Hymotion battery system for providing the power needed to run at subfreezing temperatures in a charge-depleting operation. Because of conversion limitations in the production Escape powertrain controls, the rate of charge depletion could not be maximized, which negatively affected fuel consumption at subfreezing temperatures.

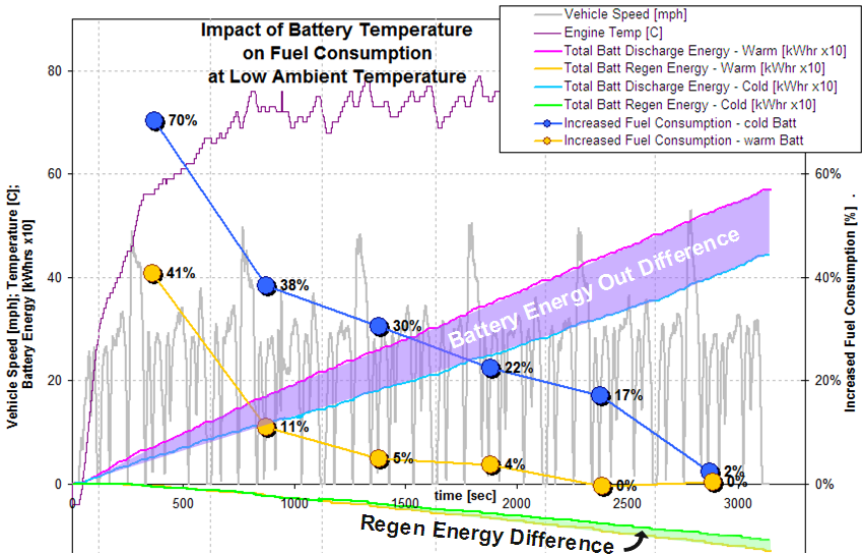

Figure 16: Battery energy differences between the two tests

4 Conclusions

The impacts of battery power and energy and of temperature were analyzed in a vehicle system context by using both hardware and software. Several conclusions were reached from the study:

- When the distance driven is higher than the all-electric range of the vehicle, the optimal control is blended: the engine is turned on at high loads throughout the trip, making the battery operate at RMS current levels lower than EV-only levels.
- The lowest fuel consumption highly depends on the available battery energy. The RMS current increases with the electrical consumption.
- Battery power moderately affects fuel consumption mostly with regard to regenerative braking energy. While the RMS current is not affected much by changes in power, downsized batteries operate more often above their continuous current limits
- When only battery temperature is considered, the AER decreases by 9% at 0°C and by 13% at 7°C, as compared with 20°C conditions. Decreases in regenerative braking energy combined with high internal-resistance losses explain the changes.
- Test results indicated that when a blended-mode vehicle is driven, the powertrain warm-up causes most of the losses during the early stage of the drive cycle, but the powertrain warms up much quicker than the battery pack, which rapidly accounts for most of the changes in fuel consumption.
- At cold temperatures, battery limitations, especially discharging energy, are the main reason for lower fuel economy.

Acknowledgments

This work was supported by DOE's FreedomCAR and Vehicle Technology Office under the direction of Lee Slezak with support and guidance from Tien Duong and Dave Howell. The submitted manuscript has been created by UChicago Argonne, LLC, Operator of Argonne National Laboratory ("Argonne"). Argonne, a U.S. Department of Energy Office of Science laboratory, is operated under Contract No. DE-AC02-06CH11357. The U.S. Government retains for itself, and others acting on its behalf, a paid-up nonexclusive, irrevocable worldwide license in said article to reproduce, prepare derivative works, distribute copies to the public, and perform publicly and display publicly, by or on behalf of the Government.

References

[1] Graham B., "Plug-in Hybrid Electric Vehicle, a Market Transformation Challenge: The DaimlerChrysler/EPRI Sprinter Van PHEV Program," 21st Electric Vehicle Symposium, April 2005.

[2] Shidore N., Pasquier M., "Interdependence of System Control and Component Sizing for a Hydrogen-fueled Hybrid Vehicle," SAE 2005-01-3457, SAE World Congress, April 2005.

[3] Karbowski D., Haliburton C., Rousseau A., "Impact of Component Size on Plug-in Hybrid Vehicles Energy Consumption Using Global Optimization," 23rd International Electric Vehicle Symposium, Anaheim, CA, Dec. 2007.

[4] Shidore N., Bohn T., "Evaluation of Cold Temperature Performance of the JCS-VL41M PHEV Battery Using Battery HIL," SAE 2008-01-1333, SAE World Congress, April 2008.

[5] Carlson R. et al., "On-road Evaluation of Advanced Hybrid Electric Vehicles over a Wide Range of Ambient Temperatures," Paper 275, 23rd International Electric Vehicle Symposium, Anaheim, CA, Dec 2007.